





Optics Letters

Extended infrared responses in Er/O-hyperdoped Si at room temperature

KUN ZHANG,^{1,2,3,†} JIAJING HE,^{4,†} TING HE,^{1,3,5,*} QING LI,^{1,3,5} MENG PENG,¹ JIAXIANG GUO,^{1,3} TAO ZHANG,^{1,3} XIAOMING WANG,⁴ HUIMIN WEN,⁴ HE ZHU,⁵ NING LI,^{3,5} PENG WANG,^{1,3} YAPING DAN,^{4,6}  AND WEIDA HU^{1,3,5} 

¹State Key Laboratory of Infrared Physics, Shanghai Institute of Technical Physics, Chinese Academy of Sciences, Shanghai 200083, China

²School of Physical Science and Technology, ShanghaiTech University, 393 Huaxia mid Road, Shanghai 201210, China

³University of Chinese Academy of Sciences, 19 Yuquan Road, Beijing 100049, China

⁴University of Michigan-Shanghai Jiao Tong University Joint Institute, Shanghai Jiao Tong University, Shanghai 200240, China

⁵Hangzhou Institute for Advanced Study, University of Chinese Academy of Sciences, Hangzhou 310024, China

⁶e-mail: yaping.dan@sjtu.edu.cn

*Corresponding author: heting@mail.sitp.ac.cn

Received 30 August 2021; revised 22 September 2021; accepted 22 September 2021; posted 23 September 2021 (Doc. ID 441553); published 8 October 2021

Silicon photonics has become the preferred candidate for technologies applicable to multifarious fields. However, the applications are strictly limited by the intrinsic in-band photo effect of silicon. Herein, near-infrared photodetectors that break through the silicon bandgap by Er/O hyperdoping are fabricated, potentially extending their applications into telecommunications, low-light-level night vision, medical treatment, and others. Er/O-hyperdoped silicon was achieved as an infrared light absorption layer through ion implantation. The lattice damage caused by ion implantation was repaired by a deep cooling process in which high-temperature samples were cooled by helium flushing cooled by liquid nitrogen. Traditional junction and metallization processes were performed to form a photodiode. We demonstrate that the device has a spectral range up to the wavelength of 1568 nm, a maximum responsivity of 165 $\mu\text{A}/\text{W}$ at 1310 nm, and 3 dB cutoff bandwidth up to 3 kHz. Finally, temperature-dependent optical-electrical characteristics were measured to demonstrate the activation mechanism of Er/O in silicon. This Letter proves silicon's potential in realizing extended infrared detection at room temperature, and it provides a possible way to fabricate infrared optoelectronics and signal processing integrated chips on a CMOS (complementary metal-oxide-semiconductor) platform. © 2021 Optical Society of America

<https://doi.org/10.1364/OL.441553>

For many years, infrared detection systems required a high operating temperature, a mature material growth technology, and a low-price fabrication process [1,2]. The commercial detectors based on InGaAs, InSb, and HgCdTe [3–9] can meet the requirements for high performance. However, they can hardly be integrated on silicon chips. Compared with these materials, silicon-based photodetectors can easily satisfy the requirements of cost-effective, environmentally friendly applications and

are compatible with on-chip Complementary-Metal-Oxide-Semiconductor (CMOS) photonic systems [10]. The challenge for silicon-based photodetectors is the silicon bandgap (about 1.12 eV), which strictly limits its applications in the near-infrared range (over ~ 1100 nm). Therefore, broadening the detection wavelength range and improving the extrinsic quantum efficiency of Si-based photodetectors in the near-infrared range through the bandgap have become significant tasks and aroused the interest of researchers. Extrinsic silicon-based infrared detectors, through doping with Group III and Group V impurities [11–13], have been fabricated and applied to many famous astronomical telescopes because of its capacity for mid- or far-infrared detection. However, the detectors can only work at temperatures below 40 K because shallow impurity levels will thermally ionize at high temperatures. The advantages of silicon-based photodetectors are drastically reduced.

In recent years, hyperdoped silicon has garnered much attention due to its prospective room temperature operating ability in the extending infrared range [14–18]. Hyperdoped silicon, using deep level dopants (with higher thermal ionization energy), will form plentiful impurity state densities to enhance photodetection in the near-infrared range [19–22]. Erbium is one of the rare earth elements that has many remarkable characteristics. Erbium-doped silicon can transfer energy between semiconductor electronic systems and the internal $4f$ state of Er ions [23]. It is worth noting that Erbium-doped silicon can induce luminescence, for which photoluminescence (PL) and electroluminescence at room temperature have been reported [24–26]. However, there is little research on the near-infrared photoelectronic response of Er-hyperdoped Si.

In this Letter, we report the realization of hyperdoped Si with an Er/O concentration up to 10^{21} cm^{-3} using an ion implantation and deep cooling annealing process. The Er/O co-doped Si PN photodiode can have a spectral range of up to 1568 nm at room temperature and a responsivity of up to 165 $\mu\text{A}/\text{W}$ at 1310 nm. This work indicates the potential of Er-doped silicon

in infrared detection at room temperature and lays a foundation for chips integrated with infrared photodetectors, LEDs, and even signal processing circuits under variable circumstances.

After surface cleaning the Si wafers, ion implantation of erbium, oxygen, and boron was completed by a high-energy ion implanter. In this way, a vertical PN junction is formed with the shallower n -type Er/O layer and the deeper p -type B layer. Deep cooling of the silicon sample was finished in an upgraded dilatometer. The samples were heated to 950°C for 5 min, followed by flushing the samples with high-purity helium cooled by liquid nitrogen. The sample was cooled to room temperature in less than 5 s through this progress. After the deep cooling treatment, the erbium, the oxygen, and the boron ions can be simultaneously activated. Then, a pair of coaxial electrodes were prepared for the PN junction.

Figure 1(a) shows the schematic diagram of the Si: Er/O photodetector. The detector has a vertical PN junction with the Er/O-doped Si as the n -type region and the B-doped Si as the p -type region. The PN junction diode is in contact with Cr/Au (10/100 nm) electrodes that were thermally evaporated. Figure 1(b) shows the room temperature current versus voltage (I - V) characteristics of the Si: Er/O devices in the dark and under light illumination. Surprisingly, the diode shows a large current when the PN junction is reverse biased [$V_b > 0$ in Fig. 1(b)]. In comparison with the forward bias ($V_b < 0$), the reverse-biased PN junction exhibits a much larger photocurrent at a level of microampere even under the illumination of sub-bandgap photons ($\lambda = 1310$ nm and 1550 nm). This is likely because the depletion region under reverse bias ($V_b > 0$) will extend more into the n -type Er/O-Si, which is sensitive to sub-bandgap photons. As shown in the inset of Fig. 1(b), the device exhibits a positive open-circuit voltage, indicating that a rectifying diode indeed exists in the device.

Temperature-dependent dark (black) and photo (red) IV characteristics were investigated as shown in Fig. 1(c). At a fixed bias of $V_b = 2$ V, the dark current and photocurrent, as a function of temperature, is presented in the Arrhenius plot, as shown in Fig. 1(d). The dark current exponentially decreases as $1000/T$

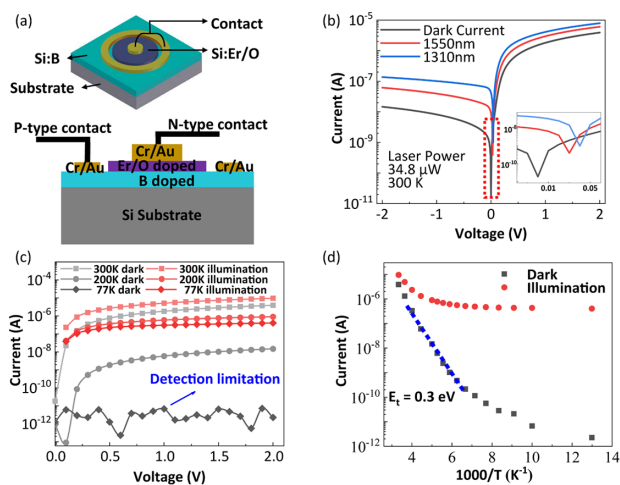


Fig. 1. (a) Schematic diagram of the three-dimensional structure and longitudinal section of the device. (b) I - V curves of PN junction in the dark (black curve) and under irradiation (the blue curve is 1310 nm, and the red curve is 1550 nm) at 300 K. The inset shows the open-circuit voltage. (c) Temperature-dependent I - V curves in the dark and under 1310 nm laser irradiation. (d) Arrhenius plot of the device under dark and illumination conditions. ($\lambda = 1550$ nm).

linearly increases (temperature drop). For a PN junction diode, the dark current comes from the thermal generation via defects in the bandgap following Eq. (1):

$$J_{\text{dark}} = q W_{\text{dep}} C_p N_t N_v \exp\left(\frac{E_v - E_t}{kT}\right), \quad (1)$$

where q is the unit charge, W_{dep} is the width of the depletion region, C_p is the hole capture cross-section, N_t is the concentration of defects, N_v is the carrier concentration related to the valence band, E_v is the valence band edge, E_t is the defect energy level, k is the Boltzmann constant, and T is the temperature. According to Eq. (1), the dark current is dominated by the exponential term and therefore potentially dependent on $1/T$, from which we can extract $E_t - E_v = 0.3$ eV. When the temperature T decreases, the exponential term will become negligibly smaller in comparison with N_v (see Eq. (S1) in Supplement 1). Therefore, Eq. (1) can be regarded as a power function of temperature, which results in the dark current starting to level off at a temperature lower than ~ 150 K [Fig. 1(d)].

To better understand how the Er-doped Si photodiode operated, the photocurrent mapping was performed with the device packed in Dewar. Figure 2(a) is an optical microscopic image of the device. The inner circular Al electrode (200 μm in radius) is in contact with the Er/O-doped region, which is the n -type. The outer concentric Al ring (600 μm in radius) is in contact with the bottom B-doped Si layer after the top Er/O-doped layer is etched by a reactive ion etch. The side view of the device is shown in Fig. 1(a). Figures 2(b) and 2(c) show the response of the device under infrared laser illumination ($\lambda = 1550$ nm). For comparison, the PN junction that is not Er/O-doped has no response to the 1550 nm laser (see Fig. S2). This demonstrates that the Er/O-doped silicon is infrared sensitive. Note that the response of the device is not spatially uniform in the Er/O-doped region. It may be caused by the nonuniformity of the Er/O doping. What is more, the image quality at 77 K is better than that at 300 K, which is due to the improved signal-to-noise ratio (SNR) at low temperatures. Indeed, although the device response attenuates at a low temperature, the dark current is significantly suppressed, as shown in Fig. 1(d), which results in the improved SNR.

Responsivity and detectivity, as important performance parameters of infrared detectors, are also important research contents of the Er-doped Si device. Figure 3(a) shows the dependence of photocurrent and responsivity on laser intensity at room temperature (300 K). The photocurrent increases sub-linearly with the laser intensity, resulting in the sub-linear decrease in responsivity. At low laser intensity, the responsivity reaches a maximum value of 165 $\mu\text{A}/\text{W}$. The responsivity increases slightly when the laser intensity decreases, which

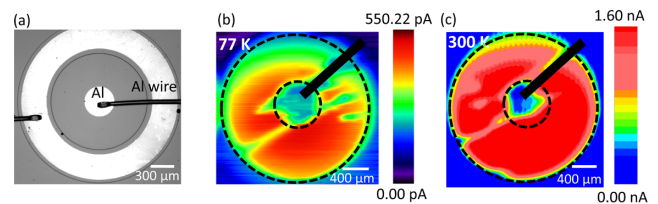


Fig. 2. (a) Microscope image of the device. Photocurrent mapping of the device at the temperatures of (b) 77 K and (c) 300 K. ($\lambda = 1550$ nm).

means the photodetectors can perform better under weak illumination. This phenomenon can be explained by the limited erbium concentration in the silicon. The photocurrent with the sub-bandgap illumination is found to scale linearly in a log–log representation with a slope of 0.938 (77 K) and 0.868 (300 K), respectively. The linear relation suggests that the response of the photodiodes is caused by the single-photon absorption process mediated by the intermediate band rather than the two-photon absorption process [27–30]. Figure 3(b) shows the photocurrent with laser intensity at different temperatures. As shown in Fig. 1(d), the dark current decreases from 5 μA to 2 pA when the temperature decreases from room temperature (300 K) to 77 K, while the photocurrent decreases by only 10 times. The noise equivalent power (NEP) can reach the minimum value of about 200 nW ($= I_{\text{dark}}/R_{\text{max}}$) at 77 K. In addition, the higher slope at low temperature is mainly caused by the increase of the minority carrier lifetime. At higher temperatures, the photo-generated carriers have more probability of being trapped by the non-radiative recombination centers, which cannot contribute to the Auger process or to the absorption of another photon to jump to the conduction band of silicon.

Figure 3(c) shows the specific detectivity (D^*) for 1310 nm at different temperatures. With the increase of the temperature, D^* decreases from 1.39×10^9 to 1.49×10^7 Jones. The specific detectivity and external quantum efficiency of the device are calculated by Eqs. (2) and (3)

$$D^* = \frac{R}{i_n} \sqrt{A \Delta f} \approx \frac{R}{\sqrt{\frac{2q I_{\text{dark}}}{A}}}, \quad (2)$$

$$\eta = \frac{I_{\text{ph}}/q}{P/h\nu}, \quad (3)$$

where R is the responsivity, i_n is the equivalent noise current, A is the effective laser sensitivity area of the device, Δf is the electrical bandwidth, q is the elementary charge, and I_{dark} is the dark current. In Eq. (3), I_{ph} is the photogenerated current, P is

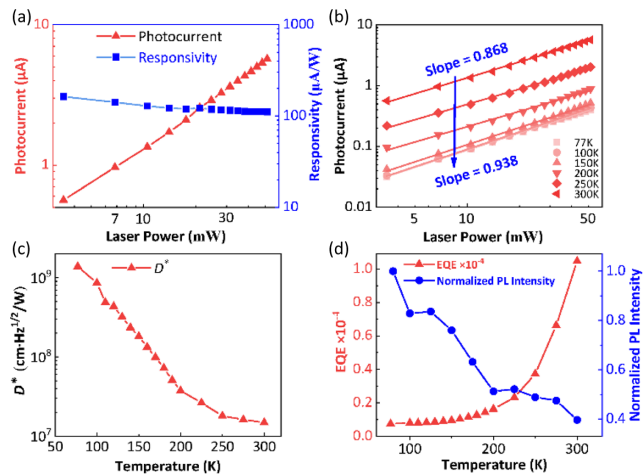


Fig. 3. (a) Measured photocurrent and calculated responsivity of the photodiodes with different laser intensities at 300 K. (b) Photocurrent versus input laser power at different temperatures. (c) Calculated specific detectivity (D^*) versus temperature. (d) Calculated external quantum efficiency (η) and normalized photoluminescence versus temperature (-1 V bias voltage, $\lambda = 1310\text{ nm}$).

the power of illumination, h is the Planck constant, and ν is the frequency of the light.

Figure 3(d) shows the calculated EQE (η) and normalized photoluminescence intensity versus temperature. With the increase of the temperature, the EQE increases from 7.44×10^{-6} to 1.05×10^{-4} , while the normalized PL intensity decreases from 1.0 to 0.4. There are several reasons that can explain this phenomenon. One reason is that the photogenerated electrons and holes can recombine at the erbium-related energy level and transfer their energy to erbium atoms. This process will excite one electron from the ground state to the excited states in the erbium. The energy has the possibility to back transfer to the silicon. With the increase of temperature, the back transfer rate can increase, which means a higher ratio of photogenerated carriers can contribute to the conductivity. This can be verified by the PL intensity of the same sample. With the increase of temperature, the PL intensity decreases about 3 times, which is called the thermal quenching process [5]. Another reason is that the increase in the concentration of non-radiative defect centers will decrease both the PL decay lifetimes and the minority carrier lifetime. The decay lifetime of the transient PL measurements shows a decreasing trend with the increase of temperature. From 77 to 150 K, the values for the minority carrier lifetime and the responsivity change only a little, while the value for the minority carrier lifetime changes very rapidly when the temperature is over 150 K and the photo responsivity increases rapidly at the same time.

Figure 4(a) shows the sub-wavelength response time of the device at 0 V. Rise time of 14 ms and fall time of 12 ms are measured. The bandwidth of our device was measured by biasing the photodiodes with -1 V and exposing it to the chopped laser of 1550 nm with a different frequency. The photocurrents are extracted by the lock-in amplifier. The 3 dB bandwidth of the photodetector can reach a frequency of 3 kHz as shown in Fig. 4(b). The bandwidth is limited by the back transfer rate of the Er-doped silicon since the deep cooling process suppresses this value. The limited value for the Er-doped silicon can reach 1 MHz [23], which provides the potential to further promote the performance of the erbium-oxygen hyperdoped silicon photodetectors. After the full-spectrum response test in the near-infrared band, the maximum wavelength is found to be 1568 nm (shown in Fig. 4(c), the higher wavelength response was limited by the SNR, and the limiting value can extend to about 4 μm according to the trap energy level), covering the 1310–1550 nm required by the field of the communication, so it can still be integrated into some CMOS circuits for image sensors.

In summary, extended infrared silicon detectors based on Er/O co-doped silicon are fabricated. The cutoff wavelength is extended to 1568 nm after the deep cooling process, and

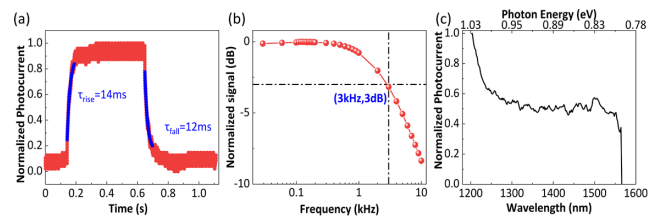


Fig. 4. (a) Response time of Si:Er/O photodetector under 1310 nm laser. (b) Normalized photocurrent at different modulation frequencies. (c) Normalized photocurrent versus the wavelength of the illumination.

the maximum detectivity reaches as high as 1.39×10^9 Jones. Extended infrared response on the Er/O-hyperdoped Si PN photodiodes related to the Er defect levels in Si has been shown. What is commendable is that it can work at room temperature. This indicates that it has broadened the all-silicon applications in the field of IR optical communication and imaging. This Letter provides new ideas for the application of all-silicon devices and plays a certain role in promoting their development.

Funding. Special-Key Project of the “Innovative Research Plan”, Shanghai Municipality Bureau of Education (2019-01-07-00-02-E00075); Foundation of Science and Technology Commission of Shanghai Municipality (19XD1404100, 21ZR1473400); China National Postdoctoral Program for Innovative Talents (BX20200205); China Postdoctoral Science Foundation (2020TQ0331); National Natural Science Foundation of China (62104053).

Acknowledgment. The devices were fabricated at the Center for Advanced Electronic Materials and Devices (AEMD) Shanghai Jiao Tong University.

Disclosures. The authors declare no conflicts of interest.

Data Availability. Data underlying the results presented in this Letter are not publicly available at this time but may be obtained from the authors upon reasonable request.

Supplemental document. See [Supplement 1](#) for supporting content.

[†]These authors contributed equally to this Letter.

REFERENCES

- S. Chen, A. Z. Weitemier, X. Zeng, L. He, X. Wang, Y. Tao, A. J. Y. Huang, Y. Hashimoto, M. Kano, H. Iwasaki, L. K. Parajuli, S. Okabe, D. B. L. Teh, A. H. All, I. Tsutsui-Kimura, K. F. Tanaka, X. Liu, and T. J. McHugh, *Science* **359**, 679 (2018).
- X. Sun, T. Zhang, L. Yu, L. Xu, and J. Wang, *Sci. Rep.* **9**, 19752 (2019).
- P. Wang, H. Xia, Q. Li, F. Wang, L. Zhang, T. Li, P. Martyniuk, A. Rogalski, and W. Hu, *Small* **15**, 1904396 (2019).
- M. R. M. Atalla, S. Assali, A. Attiaoui, C. Lemieux-Leduc, A. Kumar, S. Abdi, and O. Moutanabbir, *Adv. Funct. Mater.* **31**, 2006329 (2021).
- E. Delli, P. D. Hodgson, M. Bentley, E. Repiso, A. P. Craig, Q. Lu, R. Beanland, A. R. J. Marshall, A. Krier, and P. J. Carrington, *Appl. Phys. Lett.* **117**, 131103 (2020).
- Y. Wang, S. Dev, F. Yang, L. Nordin, Y. Wang, A. Briggs, M. Allen, J. Allen, E. Tutuc, and D. Wasserman, *Infrared Phys. Technol.* **109**, 103390 (2020).
- H. Manis-Levy, R. Shikler, Y. Golan, and G. Sarusi, *Appl. Phys. Lett.* **117**, 081107 (2020).
- N. M. Haegel, in *Quantum Sensing: Evolution and Revolution from Past to Future*, M. Razeghi and G. J. Brown, eds. (2003), pp. 182–194.
- X. Wang, B. Wang, L. Hou, W. Xie, X. Chen, and M. Pan, *Opt. Quantum Electron.* **47**, 1347 (2015).
- A. Luque, A. Marti, and C. Stanley, *Nat. Photonics* **6**, 146 (2012).
- Y. Chen, B. Wang, Y. Zang, C. Zhang, H. Zhang, Y. Yuan, D. Zhou, L. Hou, M. Pan, and X. Wang, *IEEE J. Quantum Electron.* **56**, 1 (2020).
- P. Rauter, T. Fromherz, S. Winnerl, M. Zier, A. Kolitsch, M. Helm, and G. Bauer, *Appl. Phys. Lett.* **93**, 261104 (2008).
- P. J. Love, A. W. Hoffman, N. A. Lum, K. J. Ando, W. D. Ritchie, N. J. Therrien, A. G. Toth, and R. S. Holcombe, in *Optical and Infrared Detectors for Astronomy*, J. D. Garnett and J. W. Beletic, eds. (2004), pp. 86–96.
- J. P. Mailoa, A. J. Akey, C. B. Simmons, D. Hutchinson, J. Mathews, J. T. Sullivan, D. Recht, M. T. Winkler, J. S. Williams, J. M. Warrender, P. D. Persans, M. J. Aziz, and T. Buonassisi, *Nat. Commun.* **5**, 3011 (2014).
- R. Chen, B. Fan, M. Pan, Q. Cheng, and C. Chen, *Mater. Lett.* **163**, 90 (2016).
- E. García-Hemme, R. García-Hernansanz, J. Olea, D. Pastor, A. del Prado, I. Mártel, and G. González-Díaz, *Appl. Phys. Lett.* **104**, 211105 (2014).
- M.-J. Sher, Y.-T. Lin, M. T. Winkler, E. Mazur, C. Pruner, and A. Asenbaum, *J. Appl. Phys.* **113**, 063520 (2013).
- M. Wang, Y. Berencén, E. García-Hemme, S. Prucnal, R. Hübner, Y. Yuan, C. Xu, L. Rebohle, R. Böettger, R. Heller, H. Schneider, W. Skorupa, M. Helm, and S. Zhou, *Phys. Rev. Appl.* **10**, 024054 (2018).
- X.-L. Liu, S.-X. Ma, S.-W. Zhu, Y. Zhao, X.-J. Ning, L. Zhao, and J. Zhuang, *Sens. Actuators B Chem.* **291**, 345 (2019).
- H. H. Gandhi, D. Pastor, T. T. Tran, S. Kalchmair, L. A. Smillie, J. P. Mailoa, R. Milazzo, E. Napolitani, M. Loncar, J. S. Williams, M. J. Aziz, and E. Mazur, *AIP Adv.* **10**, 075028 (2020).
- O. A. Hammadi, *Photon. Sens.* **5**, 152 (2015).
- T. Zhang, W. Ahmad, B. Liu, Y. Xuan, X. Ying, Z. Liu, Y. Li, Z. Chen, and S. Li, *Mater. Lett.* **196**, 16 (2017).
- N. Hamelin, P. G. Kik, J. F. Suyver, K. Kikoin, A. Polman, A. Schönecker, and F. W. Saris, *J. Appl. Phys.* **88**, 5381 (2000).
- P. G. Kik, M. J. A. deDood, K. Kikoin, and A. Polman, *Appl. Phys. Lett.* **70**, 1721 (1997).
- F. Priolo, G. Franzo, S. Coffa, A. Polman, S. Libertino, R. Barklie, and D. Carey, *J. Appl. Phys.* **78**, 3874 (1995).
- H. Wen, J. He, J. Hong, S. Jin, Z. Xu, H. Zhu, J. Liu, G. Sha, F. Yue, and Y. Dan, *Adv. Opt. Mater.* **8**, 2000720 (2020).
- G. Xu, X. Ren, Q. Miao, M. Yan, H. Pan, X. Chen, G. Wu, and E. Wu, *IEEE Photon. Technol. Lett.* **31**, 1944 (2019).
- D. Knez, A. M. Hanninen, R. C. Prince, E. O. Potma, and D. A. Fishman, *Light Sci. Appl.* **9**, 125 (2020).
- B. S. Nugroho, A. A. Iskandar, V. A. Malyshev, and J. Knoester, *Phys. Rev. B* **102**, 045405 (2020).
- A. Balena, M. Bianco, F. Pisano, M. Pisanello, L. Sileo, B. L. Sabatini, M. De Vittorio, and F. Pisanello, *Opt. Express* **28**, 21368 (2020).